MicroRNAs-143 and -145 induce epithelial to mesenchymal transition and modulate the expression of junction proteins

Lidia Avalle, Danny Incarnato, Aurora Savino, Marta Gai, Francesca Marino, Sara Pensa, Isaia Barbieri, Michael B. Stadler, Paolo Provero, Salvatore Oliviero, Valeria Poli

Paper: MicroRNAs-143 and -145 induce epithelial to mesenchymal transition and modulate the expression of junction proteins

CELL DEATH AND DIFFERENTIATION, 24 (10), 2017, pp: 1750-1760
DOI: 10.1038/cdd.2017.103

MicroRNAs-143 and -145 induce epithelial to mesenchymal transition by enhancing TGF-β signaling and downmodulating the expression of junction proteins

Lidia Avalle[1*], Danny Incarnato[2,3], Sara Pensa[1,4], Isaia Barbieri[1,5], Michael B. Stadler[6,7], Paolo Provero[1,8], Salvatore Oliviero[2,3], Valeria Poli[1*]

[1] Dept. of Molecular Biotechnology and Health Sciences, Molecular Biotechnology Center, University of Turin, Turin, Italy
[2] Dipartimento di Scienze della Vita e Biologia dei Sistemi, Università di Torino, Torino, Italy
[3] Human Genetics Foundation (HuGeF), via Nizza 52, 10126 Torino, Italy
[4] Present address: Dept. of Pharmacology, University of Cambridge, Cambridge, UK
[5] Present address: Gurdon Institute, University of Cambridge, Cambridge, UK
[6] Friederich Miescher Institute for Biomedical Research, Maulbeerstrasse 66, 4058 Basel, Switzerland
[7] Swiss Institute of Bioinformatics, Maulbeerstrasse 66, 4058 Basel, Switzerland
[8] Center for Translational Genomics and Bioinformatics, San Raffaele Scientific Institute, Milan, Italy
[*] Corresponding authors: Molecular Biotechnology Center, Via Nizza 52, 10126 Turin, Italy; Tel.: +39-011-6706428; valeria.poli@unito.it, lidia.avalle@unito.it

Running title:
MiRs-143/145 enhance TGFβ signaling to induce EMT

ABSTRACT

Transforming growth factor β (TGF-β) is one of the major inducers of epithelial to mesenchymal transition (EMT), a crucial program that plays a critical role in promoting carcinoma's metastasis formation. MicroRNAs-143 and -145, which are both TGF-β direct transcriptional targets, are essential for the differentiation of vascular smooth muscle cells (VSMC) during embryogenesis, a TGF-β-dependent process reminiscent of EMT. Their role in adult tissues is however less well defined and even ambiguous, since their expression was correlated both positively and negatively with tumor progression.

Here we show that high expression of both miRs-143 and -145 in mouse mammary tumor cells expressing constitutively active STAT3 (S3C) is at least partly responsible for their disrupted cell-cell junctions. Additionally, miR-143 appears to play a unique role in tumorigenesis by enhancing cell migration *in vitro* and extravasation *in vivo* while impairing anchorage-independent growth, which may explain the contradictory reports about its role in tumors.

Accordingly, we demonstrate that overexpression of either miRNA in the non-transformed mammary epithelial NMuMG cells leads to upregulation of EMT markers and increased motility. This correlates with enhanced basal and TGF-β-induced activity of SMAD transcription factors, suggesting that promotion of TGF-β mediated EMT occurs via a positive feedback loop. Moreover, pervasive transcriptome perturbations consistent with the described phenotype were observed. In particular, the expression of several transcription factors involved in the mitogenic responses, of MAPK family members and, importantly, of several tight junction proteins and the SMAD co-repressor TGIF was significantly reduced.

Our results provide important mechanistic insight into the non-redundant role played by miRs-143 and -145 in EMT-related processes in both transformed and non-transformed cells,

suggesting moreover that their expression must be finely coordinated to warrant optimal migration/invasion while not interfering with cell growth.

INTRODUCTION

Metastases at distant sites represent the main cause of death for cancer patients, underlining the importance of unravelling the molecular mechanisms that govern cancer progression to metastasis. Local invasion is an essential step in the metastasis process, and it is controlled by a coordinated series of cellular and molecular events known as EMT (1), which endows cells with enhanced migration and invasion potential, resistance to anoikis and production of extra cellular matrix components(2), facilitating the invasion at both local and distant tissues. Successful colonization of the target tissue occurs thanks to the inverse process, i.e. mesenchymal to epithelial transition, leading to the formation of metastases with features of the tumor/tissue of origin (3). EMT main outcome is the acquisition of a spindle-like morphology due to the remodeling of the actin cytoskeleton to form stress fibers, a progressive loss of epithelial-specific adhesion molecules, like E-cadherin, Zonula Occludens-1 (ZO1) and Integrin β-1, and the expression of mesenchymal-specific adhesion and cytoskeletal proteins such as N-cadherin and Vimentin (2). This process is orchestrated by the upregulation of a number of EMT-inducing transcription factors and the modulation of specific miRNAs (4-6).

TGF-β, a main inducer of EMT, plays a dual role in cancer progression. While its cytostatic activity initially inhibits proliferation of tumor cells, EMT induction favours progression to metastatic diseases. Via its complex and highly modulated signaling network, TGF-β leads to the phosphorylation and activation of SMAD factors that in turn contribute to the activation or repression of hundreds of targets, both coding and non-coding (3, 7). Among others, TGF-β was shown to strongly induce the expression of miRNAs-143 and -145, which are clustered at an

intergenic locus and subjected to coordinated transcriptional regulation (8, 9). Both were shown to play a role in the differentiation of VSMC during development (8, 10), and their expression was sufficient to induce the differentiation of multipotent neural crest stem cells into VSMCs, a TGF-β-dependent process considered as a form of EMT (8, 10, 11). In adult tissues, inactivation of both miRNAs lead to impaired neointima formation upon vascular injury, due to disorganized actin stress fibers and reduced migratory ability of smooth muscle cells.

Despite related biological functions, these two miRNAs do not share sequence similarity and mostly recognize different sets of target genes (11). They are both considered as oncosuppressors, since they are frequently downregulated in epithelial tumors such as colon (12), prostate (13) and ovary (14, 15) cancer, as well as in B-cell malignancies (16). Additionally, their locus is often deleted in tumors (17), and they both have been shown to exert anti-proliferative activities (18-22). Recently however, several reports have challenged this concept for both miR-143 and miR-145, whose expression was shown to correlate with invasion, disease grade and progression in specific types of tumors (23-26), suggesting that their role in cancer may vary according to cell type and tumor stage, similar to what has been described for TGF-β itself (27).

Here, we show that miRNAs-143 and -145 contribute to the invasive phenotype of cells derived from STAT3C/NeuT transgenic mice mammary tumors. These tumors, which develop thanks to the ectopic expression of the rat Neu oncogene in the mammary epithelium, are more aggressive and invasive when mice also carry a constitutively active form of the transcription factor STAT3 (S3C) (28). Moreover, we show that miR-143 and -145 overexpression triggers EMT features in the non-transformed NMuMG mammary epithelial cells, eliciting global gene expression changes.

RESULTS

1. MiRNAs-143 and -145 contribute to the EMT phenotype of S3C mammary tumor cells.

S3C cell lines from mammary tumors of NeuT-STAT3C transgenic mice, which express the MMTV-driven rat NeuT oncogene in the mammary epithelium and carry a knocked-in constitutively active form of the transcription factor STAT3, display enhanced migration, invasion and *in vivo* tumorigenic potential correlating with disorganized cell-cell contacts, including delocalization of the tight junctions component ZO1 (28). Accordingly, these cells also exhibit strongly increased expression of the EMT markers N-cadherin, Snail and α-SMA, and slight decreased ZO1 levels (Figure 1a), suggesting transition towards a mesenchymal status. In search for potential mediators of this phenotype, we observed that miRNAs-143 and -145 are dramatically upregulated in STAT3C cells (Figure 1b and Supplementary Figures S1a and b). To assess the potential contribution of miR-143 and -145 to the EMT status of S3C cells, we decided to interfere with their activity by means of sponge constructs. Lentiviral vectors were engineered to carry a GFP expression cassette displaying multimerized miR-143 or miR-145 target sites in their 3'UTR regions (Supplementary Figures S2a and b). Upon stable transduction of S3C cells, both sponge vectors caused a reduction of GFP levels, demonstrating their efficacy, and could revert the cell junction defects of S3C cells, triggering relocalization of both β-catenin and ZO1 to the cell membrane and leading to a more organized, epithelial-like morphology (Figure 1c). Accordingly, both miR-143 and miR-145 sponges triggered a decrease in N-cadherin and Snail and an increase in ZO1 levels (Figure 1d). These changes correlated with impaired migration as measured by Transwell assay (Figure 1e). Therefore, both miR-143 and -145 appear to be involved in regulating cell-cell contacts leading, in the case of miR-143, to significantly enhanced *in vitro* cell migration. We thus decided to extend miR-143 analysis to *in vivo* assays.

2. Interference with miRNA-143 activity impairs *in vivo* cell extravasation.

The effects of miR-143 on *in vivo* tumorigenic potential were assessed by comparing the ability of sponged or control S3C cells to extravasate into the lung parenchyma upon i.v. injection. Cells were labelled with a fluorescent dye (CMRA) allowing cell tracking and injected in the tail vein of NSG immunocompromised mice, followed by evaluation of the number of cells in the tissue at different time points. Confirming equivalent loading, comparable numbers of both cell types were observed in the lungs 15 minutes after injection, predominantly still associated to the blood vessels (Figure 2a, upper panel). Quantification after 24 hours showed significantly less cells in the lung parenchyma of mice injected with sponged S3C cells (Figure 2a, lower panel). Thus, interfering with miR-143 activity in S3C cells impairs extravasation *in vivo*. Despite this, sp-miR143 S3C cells could give rise to an equivalent number of metastases as compared with the control GFP cells (Figure 2b), suggesting that a higher percentage of sp-miR143 S3C extravasated cells are able to survive and proliferate in the lung parenchyma. Accordingly, miR-143 inhibition significantly enhanced anchorage-independent growth, as shown by the increased number and size of sp-miR143 S3C soft agar colonies (Figure 2c) and despite normal proliferation rates of adherent cells and equivalent sensitivity to anoikis (Supplementary Figures S3a and b). Enhanced anchorage-independent proliferation could therefore counterbalance the impaired extravasation leading to unaltered metastasis number. These results suggest a dual role in the metastatic process for miRNA-143, which on one hand enhances cell extravasation while on the other hand impairs the proliferation of extravasated cells.

3. MiRNAs-143 and -145 expression in mammary epithelial cells and in mammary tumor cell lines is induced by TGF-β

To confirm the involvement of miR-143 and -145 in the induction of EMT, we tested their activity in the epithelial mammary gland Namru Murine Mammary Gland (NMuMG) cell line model of TGF-β-induced EMT (29). Indeed, treatment of NMuMG cells with TGF-β for 3 days triggered a

transition to a mesenchymal-like morphology and the formation of abundant actin stress fibers (Figure 3a). As expected, TGF-β treatment elicited SMAD2 phosphorylation and reciprocal changes in the expression of N-cadherin and E-cadherin, particularly evident at 72 hours (Figure 3b). Under these conditions, we also observed a strong upregulation of the expression of both miR-143 and -145, already evident after 24 hours of stimulation and peaking at 72 hours (Figures 3c and d). Thus, miRNAs-143 and -145 are *bona fide* TGF-β targets in NMuMG cells, and their induction profiles are consistent with them playing a role in TGF-β-mediated EMT.

4. Overexpression of miRNAs-143 and -145 in NMuMG cells suppresses ZO1 expression and induces EMT.

To assess their role in TGF-β-induced EMT, both miRNA-143 and -145 were stably over-expressed together with a RFP cassette in NMuMG cells by means of lentiviral vectors (Supplementary Figures S4a and b). Overexpression of either miRNA triggered a transition in cell morphology and the formation of long, filamentous pseudopods, while cell proliferation was not altered as compared to control cells transduced with an empty vector (Figures 4a and b). Importantly, both miRNAs also triggered the upregulation of the N-cadherin and Snail EMT markers, a slight reduction of E-cadherin (Figure 4c), and a dramatic downregulation of ZO1 at both protein and mRNA level (Figures 4c and d). These changes correlated with significantly increased motility in a wound healing assay (Figure 4e). Thus, ectopic expression of both miRNAs can independently confer EMT features to normal mammary gland cells. The enhanced cell motility observed is at least partly due to the suppression of ZO1 expression, since shRNA-mediated ZO1 silencing was sufficient to enhance the migration of NMuMG cells (Figures 4f and g).

5. miRNAs-143 and -145 overexpression leads to increased SMAD-mediated transcription.

The above results suggest that mir-143 and miR-145 may impact on TGF-β/SMAD signaling. To verify this, we generated a SMAD-luciferase reporter construct, which was dose-dependently

activated by TGF-β upon transient transfection in NMuMG cells (Supplementary Figures S5a and b). Interestingly, basal luciferase activity of the SMAD reporter was 3.2 and 3.6 fold higher, respectively, in NMuMG cell overexpressing miRNA-143 or miRNA-145 as compared to empty vector cells (Figure 5a). This was apparently independent from the expression or phosphorylation levels of SMAD family members, which were not significantly altered (Supplementary Figures S5c and d). miRNAs overexpression was also able to amplify TGF-β-induced SMAD-dependent transcription, since TGF-β treatment elicited about a three-fold higher luciferase induction in overexpressing cells with respect to controls (Figure 5a). Conversely, sponge-mediated interference with the activity of either miRNA (Supplementary Figures S2a and b) significantly reduced TGF-β-induced reporter activity (Figure 5b), supporting the idea that TGF-β-dependent upregulation of miRNAs-143 and -145 contributes to the activation of SMAD-mediated transcription in a classical feed forward loop.

6. Overexpression of miRs-143 and 145 strongly perturbs the transcriptome of NMuMG cells

As shown above, miRNAs overexpressing NMuMG cells display remarkably similar alterations in the expression of relevant EMT-related genes, and in particular downregulation of E-cadherin and ZO1 expression, neither of which is however predicted as a common miRNA target by TargetScan and MREdictor softwares (30). We thus decided to assess the transcriptome alterations of the overexpressing cells by RNA sequence analysis. In keeping with their superimposable phenotypes, miR-143 and miR-145 overexpressing NMuMG cells displayed very similar mRNA expression profiles, with 1391 genes downregulated and 1006 genes upregulated by at least 2 fold (and adjusted p-value <0.05) as compared with control cells (Supplementary Table 1). Importantly, predicted targets of both miRNAs were significantly enriched among the down-, but not the upregulated genes, (Figures 6a and b, Supplementary Figures S6a and b). Nevertheless, the number of downmodulated genes greatly exceeded the number of common miRNA target mRNAs,

sixty according to MREdictor (Supplementary Table 2). Such a strong transcriptome perturbation may stem from the downregulation of key transcription factors such as Fos (c-Fos), Fosb, Creb, ATF, Elk4, Srf, and several Egr and C/EBP family members (Supplementary Figures S7a-c). Among these, Creb1 is a putative direct target of both miRNAs (Supplementary Table 2), and its modulation was also confirmed at the protein level along with that of c-Fos and Egr1 (Figure 6c).

KEGG analysis of downregulated genes revealed significant disruption of the MAP kinase pathway, and in particular strongly reduced levels of Map3k2 (MEKK2), Map4K5 and Mapk8ip3 kinases (Figure 6d, Supplementary Figures S6b and S7a-c). Downregulation of MEKK2 kinase, predicted as a common target of both miRNAs, correlated with significantly decreased phosphorylation of both ERK1/2 and MEK1/2 (Figures 6e and f).

Importantly, sequencing data not only confirmed downregulation of the Tjp1 (ZO1) mRNA (Figures 4c and d, Supplementary Figures S7a-c) but also unveiled a strong reduction in its tight junctions partners Tjp3 (ZO3) and Occludin, thus strengthening the role of miRNAs-143 and -145 in disrupting cell-cell junctions (Supplementary Figure S7c). Finally, we also observed significant downregulation of the well know SMAD transcriptional corepressor Tgif1 (TGIF) (Figure 6c and Supplementary Figure S7c), which may well explain the enhanced TGF-β-induced transcription observed in the miRNA over-expressing cells.

DISCUSSION

MiRNAs are well-known players in tumor transformation and progression, being able to exert both tumor suppressive and promoting roles (31-33). However, the definition of their specific functions often escapes rigid classifications, due to cell- and stage-specific effects such as differential expression, regulation and accessibility of their putative targets. miRNAs-143 and -145 are no exception to this rule. Indeed, both were initially classified as tumor-suppressors based on both expression analysis of tumors and cell lines and functional experiments (34-36). However, several recent publications suggested that their expression can also correlate with tumor progression, metastasis and recurrence in colorectal cancer, esophageal tumors and HBV-related hepatocellular carcinoma, where their functional role is confirmed by *in vitro* and *in vivo* experiments (23-25). Additionally, expression of both miRNAs was found to be much higher in mesenchymal cells, including the tumor stroma, than in epithelial cells, suggesting that the assessment of their expression in whole tumor biopsies may be misleading (35).

Our data demonstrate that miRNAs-143 and -145 contribute to promote EMT and cell migration in both transformed and non-transformed mammary gland cells, consistent with a pro-metastatic, rather than oncosuppressive, role. This function is consistent with the phenotype observed in adult smooth muscle cells from miR-143 and miR-145 null mice. These cells display defective rearrangement of the actin cytoskeleton and impaired migration upon vascular injury, consequently failing to give origin to the scar tissue known as neointima (10, 11, 37). Thus, despite a general consensus that the expression of miRNAs-143 and -145 triggers the differentiation of embryonal stem and precursor cells (38), correlating with proliferation arrest as also observed in several tumor models (18-20, 22) , their physiological function in adult tissues appears to be less well defined. Particularly intriguing is the observation that interference with miR-143 in the aggressive breast tumor S3C cells significantly reduced their ability to extravasate into the lung

parenchyma while increasing the proliferation of extravasated cells. Thus, miRNA-143 activity appears indeed to enhance the ability of cancer cells to invade distant tissues, but it likely has to be downregulated after extravasation in order to ensure optimal proliferation and colonization.

TGF-β is the major inducer of EMT, both during development and in adult cells including tumors (3). Our data suggest that both miRNAs-143 and -145 are involved in mediating at least some of the EMT features triggered by TGF-β treatment in normal mammary epithelial cells. Indeed, both miRNAs are *bona fide* SMAD-dependent TGF-β transcriptional targets (9), and their ectopic expression is sufficient to modulate several EMT markers and enhance cell migration independently of cytokine treatment. This effect is at least partly due to the ability of both miRNAs to enhance basal and TGF-β induced SMAD-dependent transcription.

RNA sequencing analysis has revealed that overexpression of either miRNA pervasively perturbs the transcriptome, in keeping with the knowledge that miRNAs can directly and indirectly modulate thousands of target genes, partly by regulating a high number of transcription factors (39, 40). Also in our cells transcription factors such as Srf and Elk4, the AP-1 family members c-Fos, Fosb and ATF3 and several Egr family members are highly represented among the downregulated genes. Although none of these is predicted as a direct miR-143 and/or miR-145 target, several are transcriptionally regulated by Creb1 (41), which is instead a putative direct target of both miRNAs and is also downregulated in the overexpressing cells (see also the scheme in Fig. 6g). On the other hand, Creb1 is the main transcriptional activator of Occludin, and is predicted to play a role in the transcription of Tjp1/ZO1 as well, whose promoter additionally carries several functional AP-1 binding sites (42, 43) . Thus, the reduced levels of Creb1 and of AP-1 family members may explain the observed downregulation of the mRNAs encoding for the tight junction proteins ZO1, Occludin and possibly also ZO3. In turn, altered expression of tight junction proteins can at least partly account for the enhanced migration elicited by the two miRNAs in NMuMG cells, as confirmed by

the enhanced motility of ZO1-silenced NMuMG cells.

In agreement with previous work demonstrating that miRNAs-143 and -145 can modulate MAPK signaling by targeting several genes in the signaling cascade (44), our results revealed significant disruption of the MAPK pathway. Indeed, downregulation of the putative direct common target MEKK2 (and possibly of Map4k5 and Mapk8ip3) correlates with decreased phosphorylation of both ERK1/2 and MEK1/2, without affecting their protein levels. This can in turn contribute to the observed reduced expression of the AP-1- and Srf-family transcription factors. Although the activity of MAP kinases is generally considered as a marker of proliferation and tumor transformation, the many feedback interactions with other important signaling pathways forbid simplistic interpretations. For example, Kim et al reported that miR26a-mediated downregulation of MEKK2 enhances the growth of glioblastoma cells both *in vitro* and *in vivo* (45). On the other hand, reduced basal ERK activation may well explain the impaired anchorage-independent growth of the S3C cell. In this vein, ERK-mediated phosphorylation is known to stabilize TGIF, a well-known co-repressor of SMADs transcriptional activities, thus interfering with TGF-β-mediated functions (46-48). Although Tgif1 mRNA is not predicted to be a direct miRNA target and its transcriptional regulation is poorly characterized, the observed reduced TGIF expression may very well explain the enhanced SMAD-mediated transcription, and the consequent increased migration and expression of EMT markers elicited by miR-143 and -145 overexpression.

In conclusion, our results clearly demonstrate that microRNAs -143 and -145 enhance EMT features of both transformed and normal mammary epithelial cells, increasing motility but (miR-143) impairing anchorage-independent cell proliferation. These effects occur via both direct and indirect regulation of the MAPK pathway and of transcription factors impacting on the expression of EMT markers and on TGF-β/SMADs transcriptional activity (Fig. 6g). MicroRNAs expression is known to be tightly regulated in time and space under physiological conditions, in agreement with

their ability to fine-tune gene expression. The evidences here reported support this idea, suggesting that the consequences of therapeutic approaches aimed at interfering with miRNAs activity have to be carefully evaluated.

MATERIALS AND METHODS

Ethics statement: The present investigation has been conducted in accordance with the ethical standards and according to the Declaration of Helsinki and to national and international guidelines, and has been approved by the Faculty Ethical Committee and by the Italian Ministry of Health.

Animal treatments. 12 weeks old NSG (NOD.Cg-*Prkdc*^{scid} *Il2rg*^{tm1Wjl}/SzJ) female mice were maintained in the pathogen free transgenic unit of the Molecular Biotechnology Center, under a 12 hour light-dark cycle and provided food and water *ad libitum*.

Cell lines. Murine mammary tumor cell lines (WT and S3C) were isolated from MMTV-NeuT mice and cultured as previously described (49). WT1 and S3C1 cells are used throughout the paper and referred to as WT, S3C. NMuMG cells were kindly provided by Prof. C. Watson (University of Cambridge, UK), and were maintained as previously described (29). hTGF-β1 (Peprotech, Rocky Hill, NJ, USA) was used at a final concentration of 10ng/ml for the indicated lengths of time.

Plasmid construction and generation of stable cell lines. The genomic regions containing the murine pre-miRNA-143 or -145 were amplified by PCR and cloned under the control of a CMV promoter into the pLemiR-tRFP vector (GE Healthcare, Little Chalfon, UK) to obtain the over-miR143 and over-miR145 lentiviral constructs. For the preparation of the miR-143 and miR-145 sponges, 292 nts long sequences (Supplementary Table 3), containing eight bulged target sites specific for miR-143 or miR-145 interrupted by linkers, were designed as described in Krol et al. (50), synthesized by DNA2.0 (Newark, CA, USA) and cloned in the 3'UTR of a GFP cassette in a pLenti-CMV-GFP-Puro vector (Addgene, Cambridge, MA, USA), generating the sp-miR143 and sp-miR145 vectors. The pLemiR-tRFP and pLenti-CMV-GFP-Puro empty vectors were used as controls. All stable cell lines were generated via lentiviral infection. Lentiviral particles were produced according to Trono's lab protocol (http://tronolab.epfl.ch). Supernatant was harvested 48h post-transfection, filtered with 0.45 mm filters, diluted and used to transduce cells, in the presence of

Polybrene (Sigma Aldrich, Saint Louis, MI, USA). For the transduction of S3C cells, lentiviral particles were concentrated by supernatant ultracentrifugation ($5x10^4$g for 2h at 4°C), resuspended in PBS and then used to transduce cells in low adhesion conditions. To generate the SMAD reporter a DNA oligonucleotide sequence containing three SMAD3-4 binding sites (51) (Supplementary Table 3) was cloned upstream of the TATA box in the pTA-Luc vector (Addgene). The SMAD reporter was co-transfected with a pRL-TK Renilla plasmid in NMuMG cells by means of Lipofectamine 2000 (Thermo Fisher Scientific, Waltham, MA, USA), according to manufacturer's instructions. Firefly and Renilla Luciferase activities were measured 48h upon transfection, with the Dual-Glo Luciferase Assay system (Promega, Madison, WI, USA) and a 96 microplates GloMax luminometer (Promega).

Western blots. Total protein extracts were obtained and Western blots performed as described in Schiavone et al (52). The following antibodies were used: N-cadherin (Abcam, Cambridge, UK); E-cadherin, β-catenin (BD, Franklin Lakes, NJ, USA); Snail, pSMAD2, SMAD2, pSMAD3-1, SMAD3, pERK1/2, ERK1/2, pMEK1/2, MEK1/2, Creb1 (Cell Signaling Technology, Danvers, MA, USA); α-SMA, α-tubulin (Sigma Aldrich); ZO1 (Thermo Fisher Scientific); SMAD4, Egr1, c-Fos, MEKK2, TGIF, Actin (Santa Cruz Biotechnology, Santa Cruz, CA, USA); GAPDH (Merck-Millipore); Vinculin and GFP (home made). Western blot chemilumiscent signals were acquired with a ChemidocTouch and analysed with the ImageLab software (BioRad). All blots were repeated at least three times. One representative image is shown.

RNA isolation and qRT-PCR for miRNA or mRNA detection. Total RNA was isolated using TRIzol Reagent (Thermo Fisher Scientific). qRT-PCR reactions for miRNA detection were performed with the indicated TaqMan MicroRNA Assay (Thermo Fisher Scientific) on total RNA, according to manufacturer's instructions, and normalized on U6 RNA levels. mRNAs expression levels were evaluated by means of qRT-PCR assays based on the Universal Probe Library (Roche, Basel,

Switzerland) technology, normalized on 18s RNA levels. Primers and probes used are listed in Supplementary Table 4. The relative expression levels between samples were calculated using the comparative delta CT (threshold cycle number) method ($2^{-\Delta\Delta CT}$) with a control sample as the reference point.

Immunofluorescence. Cells plated on glass coverslips were treated as reported in Barbieri et al. (28), incubated with primary antibodies at room temperature for 1 hour, followed by anti-rabbit or anti-mouse conjugated AlexaFluor 568 antibody (Thermo Fisher Scientific) or phalloidin-FITC (Sigma Aldrich) and then by Hoescht-dye. An Axiovert 200M Zeiss microscope or the Axio-Observer-Z1 Zeiss microscope with the ApoTome system for optical sectioning were used. Images were acquired with the MetaMorph software (Molecular Devices, Sunnivale, CA, USA) or the AxioVision release 4.6.3 software (Carl Zeiss, Oberkochen, Germany), respectively.

Scratch assay and Transwell migration assays. In vitro scratch assays were performed as described by Liang et al. (53), with some modifications. In brief, cells were grown to confluence and starved overnight with 0% FCS. Two hours before the scratch, cells were treated with 10 µg/ml mitomycin C (Sigma Aldrich). The cell monolayer was scraped in a straight line with a pipet tip in order to create a linear wound. Debris were removed by washing the cells with PBS and then replaced with complete medium plus mitomycin C. Photographs of the wounds (10 fields per experiment) were taken with a phase-contrast Olympus IX70 microscope. For each image cells migrated into the original wound were measured, normalized to the original wound area, then the control condition is imposed as reference and other conditions expressed as relative. Transwell assays were performed as described in Barbieri et al. (28), after 24h of migration pictures of the cells on the lower surface were taken and then quantified with the ImageJ software.

***In vivo* extravasation and lung metastases.** For extravasation experiments, $5x10^5$ cells were labelled with CellTracker Orange CMRA (Thermo Fisher Scientific), resuspended in PBS and

injected into the tail vein of NSG mice. After 15min or 24h, mice were sacrificed and 4% paraformaldehyde was injected into the trachea. Total lungs were dissected and photographed using a Leica MZ16F fluorescence stereomicroscope. Red-fluorescent (CMRA) cells were counted using the ImageJ software. For long term metastases, $1x10^5$ cells were resuspended in PBS and injected into the tail vein of 7-week-old female NSG mice. After 3 weeks mice were sacrificed, lungs collected and fixed for paraffin embedding, semiserial sections at 100 μm intervals were stained with H&E and neoplastic lesions quantified with the ImageJ software.

Anchorage-independent growth assay and anoikis. 1 x 10^4 cells were resuspended in complete DMEM containing 0.3% low gelling agarose (Sigma Aldrich) and seeded in plates containing a layer of solid 0.6% agar (Sigma Aldrich). After 3 weeks colonies were stained with nitroblue tetrazolium (Sigma Aldrich), photographed with a Nikon SMZ1000 stereomicroscope and colonies were counted using the ImageJ Software. For suspension-induced anoikis, confluent adherent cells were detached from regular culture plates with EDTA, seeded onto poly-HEMA coated plates (poly-HEMA, 10 mg/ml, Sigma Aldrich), and cultured for 24 hours in complete culture medium. Apoptosis was assessed by annexin V staining (BD) with aFACScalibur flow citometer (BD) and CellQuest software. Positive cells are expressed as percentage of the total.

RNA-Seq library preparation. For RNA-Seq library preparation, approximately 2 μg of total RNA from the different NMuMG cell lines was subjected to poly(A) selection, and libraries were prepared using the TruSeq RNA Sample Prep Kit (Illumina, San Diego, CA, USA) following the manufacturer's instructions. Sequencing was performed on the Illumina NextSeq 500 platform.

RNA-Seq data analysis. Illumina BCL files were demultiplexed to FastQ format using the *bcl2fastq* tool from Illumina. Prior to mapping, the reads quality was estimated using the FastQC tool v0.10.1 (http://www.bioinformatics.babraham.ac.uk/projects/fastqc/). The nucleotide positions with a quality score below 30 (Phred33 scale) were trimmed using the *fastx_trimmer* tool from the

FASTX Toolkit (http://hannonlab.cshl.edu/fastx_toolkit/). After low-quality position trimming, the reads in which sequencing continued through the 3' adapter sequence were subjected to adapter clipping using the *fastx_clipper* tool from the FASTX Toolkit, and the reads shorter than 35 nt were discarded. Reads were mapped to mouse mm9 assembly using TopHat v2 (http://tophat.cbcb.umd.edu/, parameters: --bowtie1 -a 5 --library-type fr-unstranded). Genes counts were computed using the *htseq-count* tool from the HTSeq package (http://www.huber.embl.de/HTSeq/doc/overview.html) and differential expression analysis was performed using R and DESeq2 package (http://www.bioconductor.org/packages/devel/bioc/html/DESeq2.html). Genes with adjusted p-value < 0.05 and abs(log2(Fold Change)) >= 1 were considered significantly modulated, and kept for downstream analyses.

MiRNA targets prediction. For microRNA targets prediction, we used either MREdictor (30) or TargetScan algorithms. Annotated 3'-UTRs for up- or downregulated genes in either miR-143a or miR-145a overexpressing cells, were scanned for strict miRNA targets (8mer, 7mer-m8, and 7mer-A1). The significance of the measured overlaps were calculated using a hypergeometric test.

Statistical analyses. Unless otherwise noted, data were analyzed by one-way ANOVA or Student's t-test, using the Prism (GraphPad software). For qRT-PCR statistical analyses were performed on $2^{-\Delta\Delta CT}$ values.

ACKNOWLEDGEMENTS

We wish to thank E. Monteleone for bioinformatics support, F. Orso for the generous gift of reagents and for technical advice, D. Taverna for useful discussion, M. Forni for help with histological analysis, F. Orso, D. Taverna and M. Santoro for critically reading the manuscript. This work was supported by grants from the Italian Cancer Research Association (AIRC IG 13009, 16930 to V.P., and 15217 to S.O.), the Italian Ministry of University and Research (MIUR PRIN, prot. 20129JLHSY), the Ateneo/Compagnia di San Paolo (TO_Call2_2012_0062), and the Truus and Gerrit van Riemsdijk Foundation, Lichtestein to V.P. M.B.S. was supported by the MetastasiX project of the Swiss Initiative for Systems Biology (SystemsX.ch). L.A. was the recipient of a FIRC postdoctoral fellowship.

CONFLICT OF INTEREST

The authors declare no conflict of interest.

SUPPLEMENTARY INFORMATION

Supplementary information is available at Cell Death & Differentiation's website.

BIBLIOGRAPHY

1. Peinado H, Olmeda D, Cano A. Snail, Zeb and bHLH factors in tumour progression: an alliance against the epithelial phenotype? *Nature reviews Cancer*. 2007;**7**(6):415-28.

2. Christiansen JJ, Rajasekaran AK. Reassessing epithelial to mesenchymal transition as a prerequisite for carcinoma invasion and metastasis. *Cancer Res*. 2006;**66**(17):8319-26.

3. Massague J. TGFbeta signalling in context. *Nature reviews Molecular cell biology*. 2012;**13**(10):616-30.

4. Blanco MJ, Moreno-Bueno G, Sarrio D, Locascio A, Cano A, Palacios J*, et al.* Correlation of Snail expression with histological grade and lymph node status in breast carcinomas. *Oncogene*. 2002;**21**(20):3241-6.

5. Spaderna S, Schmalhofer O, Wahlbuhl M, Dimmler A, Bauer K, Sultan A*, et al.* The transcriptional repressor ZEB1 promotes metastasis and loss of cell polarity in cancer. *Cancer Res*. 2008;**68**(2):537-44.

6. Yang J, Mani SA, Donaher JL, Ramaswamy S, Itzykson RA, Come C*, et al.* Twist, a master regulator of morphogenesis, plays an essential role in tumor metastasis. *Cell*. 2004;**117**(7):927-39.

7. Gregory PA, Bracken CP, Bert AG, Goodall GJ. MicroRNAs as regulators of epithelial-mesenchymal transition. *Cell Cycle*. 2008;**7**(20):3112-8.

8. Cordes KR, Sheehy NT, White MP, Berry EC, Morton SU, Muth AN*, et al.* miR-145 and miR-143 regulate smooth muscle cell fate and plasticity. *Nature*. 2009;**460**(7256):705-10.

9. Long X, Miano JM. Transforming growth factor-beta1 (TGF-beta1) utilizes distinct pathways for the transcriptional activation of microRNA 143/145 in human coronary artery smooth muscle cells. *The Journal of biological chemistry*. 2011;**286**(34):30119-29.

10. Elia L, Quintavalle M, Zhang J, Contu R, Cossu L, Latronico MVG*, et al.* The knockout of miR-143 and -145 alters smooth muscle cell maintenance and vascular homeostasis in mice: correlates with human disease. *Cell Death and Differentiation*. 2009:1-9.

11. Xin M, Small EM, Sutherland LB, Qi X, McAnally J, Plato CF*, et al.* MicroRNAs miR-143 and miR-145 modulate cytoskeletal dynamics and responsiveness of smooth muscle cells to injury. *Genes & Development*. 2009;**23**(18):2166-78.

12. Akao Y, Nakagawa Y, Hirata I, Iio A, Itoh T, Kojima K*, et al.* Role of anti-oncomirs miR-143 and -145 in human colorectal tumors. *Cancer gene therapy*. 2010;**17**(6):398-408.

13. Ozen M, Creighton CJ, Ozdemir M, Ittmann M. Widespread deregulation of microRNA expression in human prostate cancer. *Oncogene*. 2008;**27**(12):1788-93.

14. Nam EJ, Yoon H, Kim SW, Kim H, Kim YT, Kim JH*, et al.* MicroRNA expression profiles in serous ovarian carcinoma. *Clinical cancer research : an official journal of the American Association for Cancer Research*. 2008;**14**(9):2690-5.

15. Iorio MV, Visone R, Di Leva G, Donati V, Petrocca F, Casalini P*, et al.* MicroRNA signatures in human ovarian cancer. *Cancer Res*. 2007;**67**(18):8699-707.

16. Akao Y, Nakagawa Y, Kitade Y, Kinoshita T, Naoe T. Downregulation of microRNAs-143 and -145 in B-cell malignancies. *Cancer science*. 2007;**98**(12):1914-20.

17. Calin GA, Sevignani C, Dumitru CD, Hyslop T, Noch E, Yendamuri S*, et al.* Human microRNA genes are frequently located at fragile sites and genomic regions involved in cancers. *Proc Natl Acad Sci U S A*. 2004;**101**(9):2999-3004.

18. Spizzo R, Nicoloso MS, Lupini L, Lu Y, Fogarty J, Rossi S*, et al.* miR-145 participates with TP53 in a death-promoting regulatory loop and targets estrogen receptor-alpha in human breast cancer cells. *Cell Death Differ*. 2010;**17**(2):246-54.

19. Kent OA, Chivukula RR, Mullendore M, Wentzel EA, Feldmann G, Lee KH*, et al.* Repression of the miR-143/145 cluster by oncogenic Ras initiates a tumor-promoting feed-forward pathway. *Genes & Development*. 2010;**24**(24):2754-9.

20. Sachdeva M, Mo YY. miR-145-mediated suppression of cell growth, invasion and metastasis. *American journal of translational research*. 2010;**2**(2):170-80.

21. Sachdeva M, Zhu S, Wu F, Wu H, Walia V, Kumar S*, et al.* p53 represses c-Myc through induction of the tumor suppressor miR-145. *Proceedings of the National Academy of Sciences of the United States of America*. 2009;**106**(9):3207-12.

22. Zhang J, Sun Q, Zhang Z, Ge S, Han ZG, Chen WT. Loss of microRNA-143/145 disturbs cellular growth and apoptosis of human epithelial cancers by impairing the MDM2-p53 feedback loop. *Oncogene*. 2013;**32**(1):61-9.

23. Derouet MF, Liu G, Darling GE. MiR-145 Expression Accelerates Esophageal Adenocarcinoma Progression by Enhancing Cell Invasion and Anoikis Resistance. *PloS one*. 2014;**9**(12):e115589.

24. Zhang X, Liu S, Hu T, Liu S, He Y, Sun S. Up-regulated microRNA-143 transcribed by nuclear factor kappa B enhances hepatocarcinoma metastasis by repressing fibronectin expression. *Hepatology*. 2009;**50**(2):490-9.

25. Yuan W, Sui C, Liu Q, Tang W, An H, Ma J. Up-Regulation of MicroRNA-145 Associates with Lymph Node Metastasis in Colorectal Cancer. *PloS one*. 2014;**9**(7):e102017.

26. Wu P, Liang J, Yu F, Zhou Z, Tang J, Li K. miR-145 promotes osteosarcoma growth by reducing expression of the transcription factor friend leukemia virus integration 1. *Oncotarget*. 2016;**7**(27):42241-51.

27. Meulmeester E, Ten Dijke P. The dynamic roles of TGF-beta in cancer. *The Journal of pathology*. 2011;**223**(2):205-18.

28. Barbieri I, Pensa S, Pannellini T, Quaglino E, Maritano D, Demaria M*, et al.* Constitutively active Stat3 enhances neu-mediated migration and metastasis in mammary tumors via upregulation of Cten. *Cancer Res*. 2010;**70**(6):2558-67.

29. Robson EJ, Khaled WT, Abell K, Watson CJ. Epithelial-to-mesenchymal transition confers resistance to apoptosis in three murine mammary epithelial cell lines. *Differentiation; research in biological diversity*. 2006;**74**(5):254-64.

30. Incarnato D, Neri F, Diamanti D, Oliviero S. MREdictor: a two-step dynamic interaction model that accounts for mRNA accessibility and Pumilio binding accurately predicts microRNA targets. *Nucleic acids research*. 2013;**41**(18):8421-33.

31. Esquela-Kerscher A, Slack FJ. Oncomirs - microRNAs with a role in cancer. *Nature reviews Cancer*. 2006;**6**(4):259-69.

32. Lu J, Getz G, Miska EA, Alvarez-Saavedra E, Lamb J, Peck D*, et al.* MicroRNA expression profiles classify human cancers. *Nature*. 2005;**435**(7043):834-8.

33. Nicoloso MS, Spizzo R, Shimizu M, Rossi S, Calin GA. MicroRNAs--the micro steering wheel of tumour metastases. *Nature reviews Cancer*. 2009;**9**(4):293-302.

34. Cioce M, Strano S, Muti P, Blandino G. Mir 145/143: tumor suppressor, oncogenic microenvironmental factor or ...both? *Aging (Albany NY)*. 2016;**8**(5):1-3.

35. Kent OA, McCall MN, Cornish TC, Halushka MK. Lessons from miR-143/145: the importance of cell-type localization of miRNAs. *Nucleic acids research*. 2014;**42**(12):7528-38.

36. Zhang R, Wang L, Yang A-G. Is microRNA‐143 really a turncoat of tumor suppressor microRNA in hepatitis B virus‐related hepatocellular carcinoma? *Hepatology*. 2009;**50**(3):987-.

37. Cheng Y, Liu X, Yang J, Lin Y, Xu DZ, Lu Q*, et al.* MicroRNA-145, a novel smooth muscle cell phenotypic marker and modulator, controls vascular neointimal lesion formation. *Circulation research*. 2009;**105**(2):158-66.

38. Xu N, Papagiannakopoulos T, Pan G, Thomson JA, Kosik KS. MicroRNA-145 regulates OCT4, SOX2, and KLF4 and represses pluripotency in human embryonic stem cells. *Cell*. 2009;**137**(4):647-58.

39. Kaller M, Hermeking H. Interplay Between Transcription Factors and MicroRNAs Regulating Epithelial-Mesenchymal Transitions in Colorectal Cancer. *Adv Exp Med Biol*. 2016;**937**:71-92.

40. Lui P-Y, Jin D-Y, Stevenson NJ. MicroRNA: master controllers of intracellular signaling pathways. *Cellular and molecular life sciences : CMLS*. 2015;**72**(18):3531-42.

41. Mayr B, Montminy M. Transcriptional regulation by the phosphorylation-dependent factor CREB. *Nature reviews Molecular cell biology*. 2001;**2**(8):599-609.

42. Lui W-Y, Wong EWP, Guan Y, Lee WM. Dual transcriptional control of claudin-11 via an overlapping GATA/NF-Y motif: Positive regulation through the interaction of GATA, NF-YA, and CREB and negative regulation through the interaction of Smad, HDAC1, and mSin3A. *J Cell Physiol*. 2007;**211**(3):638-48.

43. Zhong Y, Zhang B, Eum SY, Toborek M. HIV-1 Tat Triggers Nuclear Localization of ZO-1 via Rho Signaling and cAMP Response Element-Binding Protein Activation. *Journal of Neuroscience*. 2012;**32**(1):143-50.

44. Kent OA, Fox-Talbot K, Halushka MK. RREB1 repressed miR-143/145 modulates KRAS signaling through downregulation of multiple targets. *Oncogene*. 2013;**32**(20):2576-85.

45. Kim H, Huang W, Jiang X, Pennicooke B, Park PJ, Johnson MD. Integrative genome analysis reveals an oncomir/oncogene cluster regulating glioblastoma survivorship. *Proc Natl Acad Sci U S A*. 2010;**107**(5):2183-8.

46. Horie T, Ono K, Kinoshita M, Nishi H, Nagao K, Kawamura T*, et al.* TG-interacting factor is required for the differentiation of preadipocytes. *Journal of lipid research*. 2008;**49**(6):1224-34.

47. Lo RS, Wotton D, Massague J. Epidermal growth factor signaling via Ras controls the Smad transcriptional co-repressor TGIF. *The EMBO journal*. 2001;**20**(1-2):128-36.

48. Dai C, Liu Y. Hepatocyte growth factor antagonizes the profibrotic action of TGF-beta1 in mesangial cells by stabilizing Smad transcriptional corepressor TGIF. *Journal of the American Society of Nephrology : JASN*. 2004;**15**(6):1402-12.

49. Barbieri I, Pensa S, Pannellini T, Quaglino E, Maritano D, Demaria M*, et al.* Constitutively active Stat3 enhances neu-mediated migration and metastasis in mammary tumors via upregulation of Cten. *Cancer Research*. 2010;**70**(6):2558-67.

50. Krol J, Busskamp V, Markiewicz I, Stadler MB, Ribi S, Richter J*, et al.* Characterizing light-regulated retinal microRNAs reveals rapid turnover as a common property of neuronal microRNAs. *Cell*. 2010;**141**(4):618-31.

51. Zawel L, Dai JL, Buckhaults P, Zhou S, Kinzler KW, Vogelstein B*, et al.* Human Smad3 and Smad4 are sequence-specific transcription activators. *Molecular cell*. 1998;**1**(4):611-7.

52. Schiavone D, Dewilde S, Vallania F, Turkson J, Di Cunto F, Poli V. The RhoU/Wrch1 Rho GTPase gene is a common transcriptional target of both the gp130/STAT3 and Wnt-1 pathways. *The Biochemical journal*. 2009;**421**(2):283-92.

53. Liang CC, Park AY, Guan JL. In vitro scratch assay: a convenient and inexpensive method for analysis of cell migration in vitro. *Nature protocols*. 2007;**2**(2):329-33.

FIGURE LEGENDS

Figure 1. MicroRNAs-143 and -145 modulate cell-cell contacts and migration of S3C cells. a,b) S3C and WT cells were analyzed **(a)** by Western blot with the indicated antibodies, or **(b)** by qRT-PCR to assess miRNAs expression levels. Mean ± S.E.M. of expression values relative to WT cells. N=3. **c-e)** sp-miR143, sp-miR-145 or empty vector control S3C cells were analyzed by **(c)** IF with indicated antibodies (scale bar=20μm), **(d)** Western blot with indicated antibodies and **(e)** by Transwell assay. Data are mean ± S.E.M. of the area covered by migrated cells, relative to the empty vector control. N=3.

Figure 2. MicroRNA-143 inhibition reduces extravasation but not metastases. (a) Fluorescently labelled sp-miR143 or empty vector S3C cells were injected i.v. into NSG mice (scale bar=1mm), followed by analysis of the lungs at the indicated times. Quantification at 24 hours (mean cell number ± S.E.M) is shown in the histogram. N=7. **(b)** Lung metastases were assessed three weeks after cells injection by H&E staining of whole lung sections (left panel, scale bar=5mm). Quantification is shown in the histogram and normalized to the lung area (mean± S.E.M). N=4. **(c)** Soft agar cultures are shown on the left panel, scale bar=5mm). The histograms show quantification of colony number and size (mean ± S.E.M). N=3.

Figure 3. MicroRNAs-143 and -145 are induced by TGF-β treatment.

NMuMG cells either untreated (NT) or treated with TGF-β for the indicated time were analyzed by **a)** phase contrast and immunofluorescence (scale bar=30μm), **b)** Western blot on whole cell extracts with the indicated antibody, and **(c, d)** qRT-PCR assessing miR-143 and miR-145 expression. Data are mean ± S.E.M. of expression values relative to untreated cells. N=3.

Figure 4. MicroRNAs-143 and -145 overexpression in NMuMG cells alters cell morphology and enhances cell motility. **a-e)** NMuMG cells overexpressing miR-143, miR-145 or transduced with the control empty vector were analyzed by: **a)** Fluorescence with phalloidin-FITC, showing changes in the actin cytoskeleton (scale bar=20μm). **b)** Cell proliferation assay (mean cell counts ± S.E.M; N=3), **c)** Western blot on total cell lysates, **d)** qRT-PCR measuring ZO1 mRNA (mean ± S.E.M. of the expression values relative to empty vector, N=3) and **e)** Scratch assay in a confluent cell monolayer, measured after 24 hours. The fluorescent images show the RFP-expressing cells (scale bar= 100μm), while the histogram describes the % of wound closure (see Materials and Methods section), relative to empty vector control. N=3. **f, g)** NMuMG cells were transduced with three different ZO1 shRNA vectors (shZO1 #1, 2, 3), or with a scrambled control (shSCR), and analyzed by Western blot to assess silencing **(f)**, and by scratch assay **(g)**. The histogram describes the % of wound closure relative to shSCR control at 24 hours. N=3.

Figure 5. MicroRNAs-143 and -145 enhance SMAD-dependent transcription. Luciferase activity of a SMAD-reporter sensor was assessed in NMuMG cells stimulated or not with TGF-β for 24h either **(a)** stably overexpressing the miRNAs, or **(b)** stably trasduced with miR-143 or miR-145 sponge vectors. Luciferase activity (mean ± S.E.M.) was calculated relative to untreated empty vector cells, upon Renilla normalization. N=3.

Figure 6. Overexpression of microRNA-143 or -145 profoundly perturbates the transcriptome of NMuMG cells. Venn diagrams representing statistically significant enrichment of MREdictor predicted targets of **(a)** miR-143 or **(b)** miR-145 among the genes downregulated by overexpression of both miRNAs in NMuMG cells. **c-f)** Cell lysates from the indicated cells were

analyzed with the indicated antibodies. **g)** The scheme shows a model explaining the EMT phenotype triggered by overexpression of either microRNA.

Fig.1

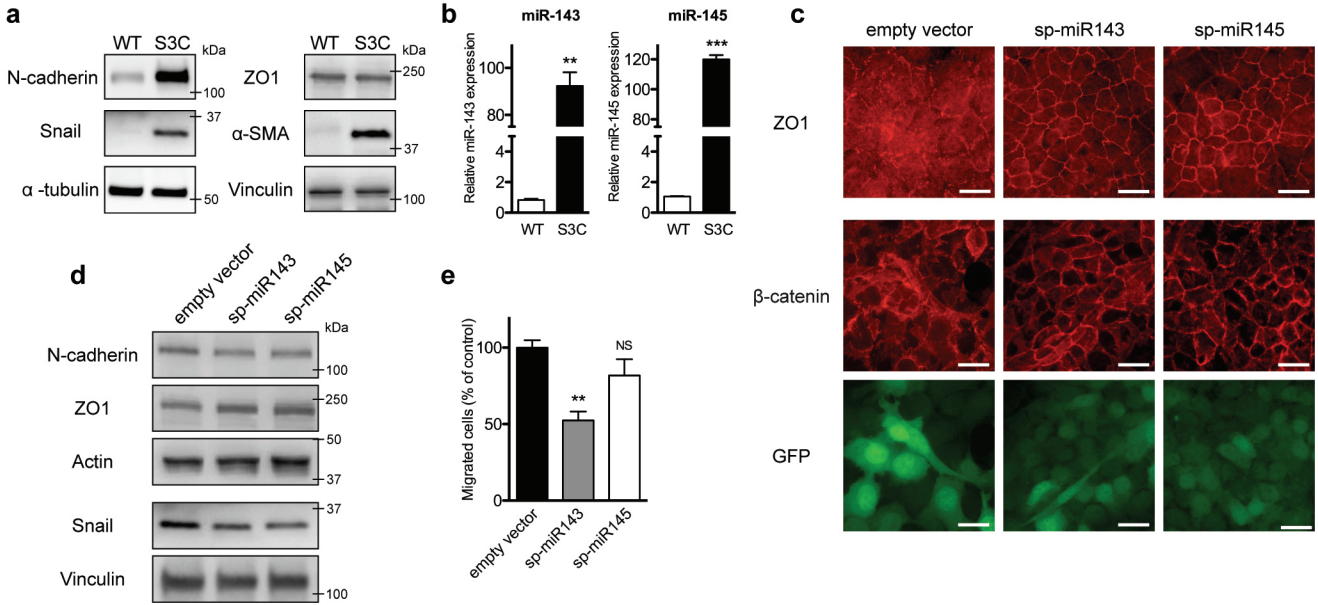
a
WT
S3C
kDa
N-cadherin
100
Snail
37
α -tubulin
50
ZO1
250
α-SMA
37
Vinculin
100
b
miR-143
miR-145
Relative miR-143 expression
Relative miR-145 expression
**
***
WT
S3C
c
empty vector
sp-miR143
sp-miR145
ZO1
β-catenin
GFP
d
empty vector
sp-miR143
sp-miR145
kDa
N-cadherin
100
ZO1
250
Actin
50
37
Snail
37
Vinculin
100
e
Migrated cells (% of control)
100
50
0
**
NS
empty vector
sp-miR143
sp-miR145

Fig.2

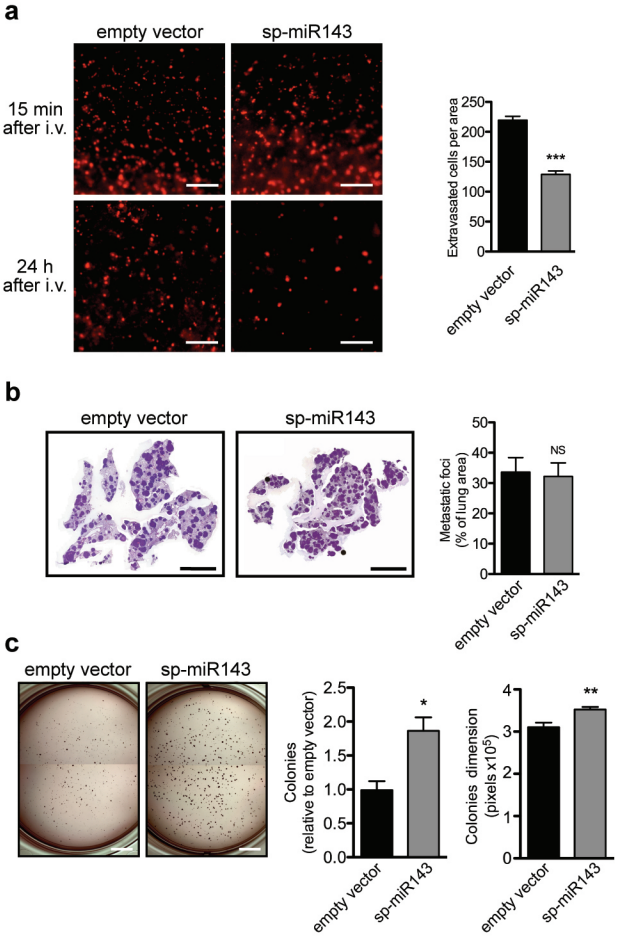
a
empty vector
sp-miR143
15 min after i.v.
24 h after i.v.
Extravasated cells per area
250
200
150
100
50
0
***
empty vector
sp-miR143
b
empty vector
sp-miR143
Metastatic foci (% of lung area)
50
40
30
20
10
0
NS
empty vector
sp-miR143
c
empty vector
sp-miR143
Colonies (relative to empty vector)
2.5
2.0
1.5
1.0
0.5
0.0
*
empty vector
sp-miR143
Colonies dimension (pixels x10³)
4
3
2
1
0
**
empty vector
sp-miR143

Fig.3

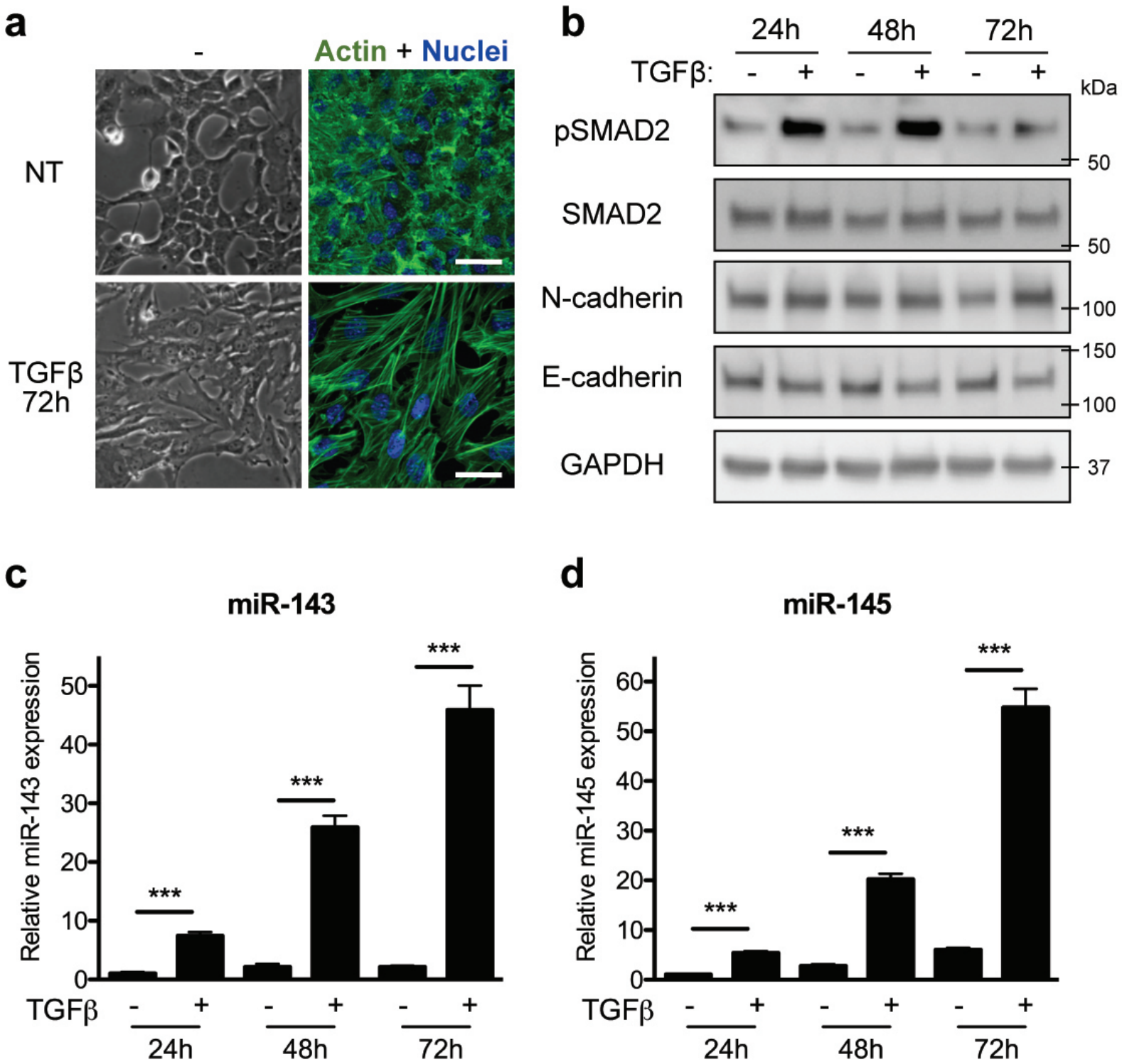
a
-
Actin + Nuclei
NT
TGFβ
72h
b
24h
48h
72h
TGFβ:
- + - + - +
kDa
pSMAD2
SMAD2
N-cadherin
E-cadherin
GAPDH
50
50
100
150
100
37
c
miR-143
Relative miR-143 expression
0
10
20
30
40
50
***
***
***
TGFβ
- + - + - +
24h
48h
72h
d
miR-145
Relative miR-145 expression
0
10
20
30
40
50
60
***
***
***
TGFβ
- + - + - +
24h
48h
72h

Fig.4

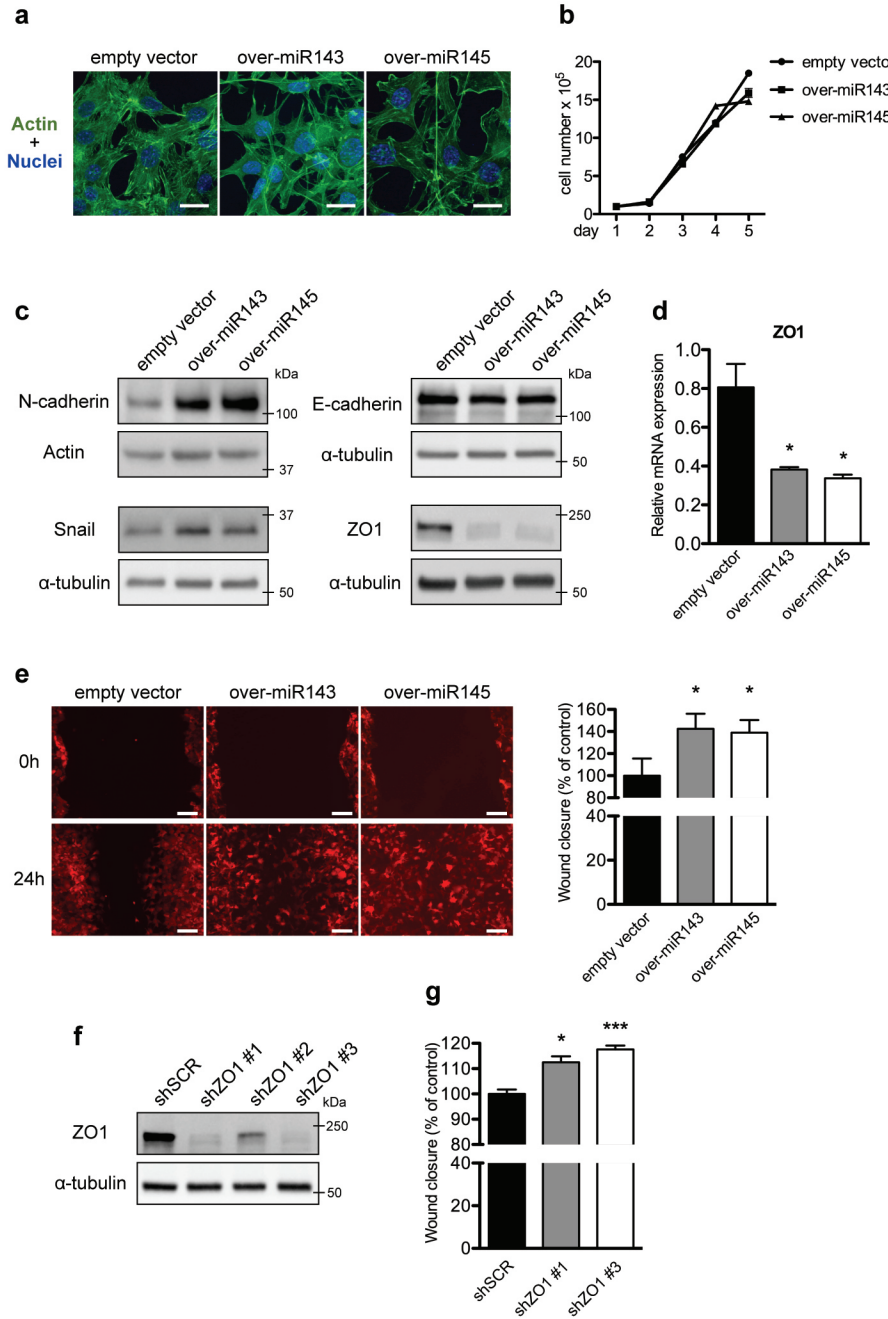
a
empty vector
over-miR143
over-miR145
Actin
+
Nuclei
b
cell number x 10^5
day
empty vector
over-miR143
over-miR145
c
empty vector
over-miR143
over-miR145
kDa
N-cadherin
Actin
Snail
α-tubulin
E-cadherin
α-tubulin
ZO1
α-tubulin
d
ZO1
Relative mRNA expression
e
empty vector
over-miR143
over-miR145
0h
24h
Wound closure (% of control)
f
shSCR
shZO1 #1
shZO1 #2
shZO1 #3
kDa
ZO1
α-tubulin
g
Wound closure (% of control)
shSCR
shZO1 #1
shZO1 #3

Fig.5

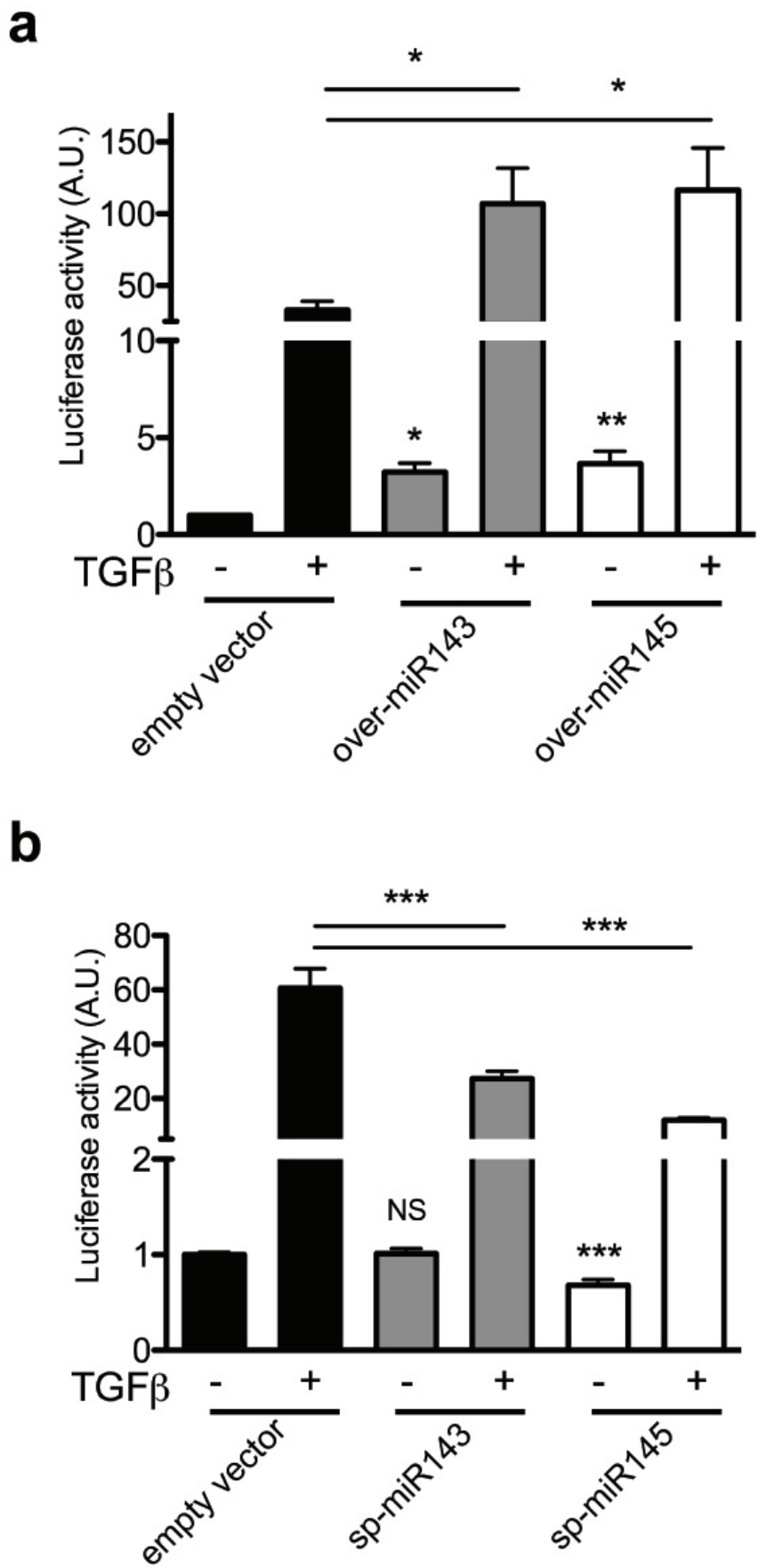
a
*
*
Luciferase activity (A.U.)
150
100
50
10
5
0
*
**
TGFβ
-
+
-
+
-
+
empty vector
over-miR143
over-miR145
b
***
***
Luciferase activity (A.U.)
80
60
40
20
2
1
0
NS
***
TGFβ
-
+
-
+
-
+
empty vector
sp-miR143
sp-miR145

Fig.6

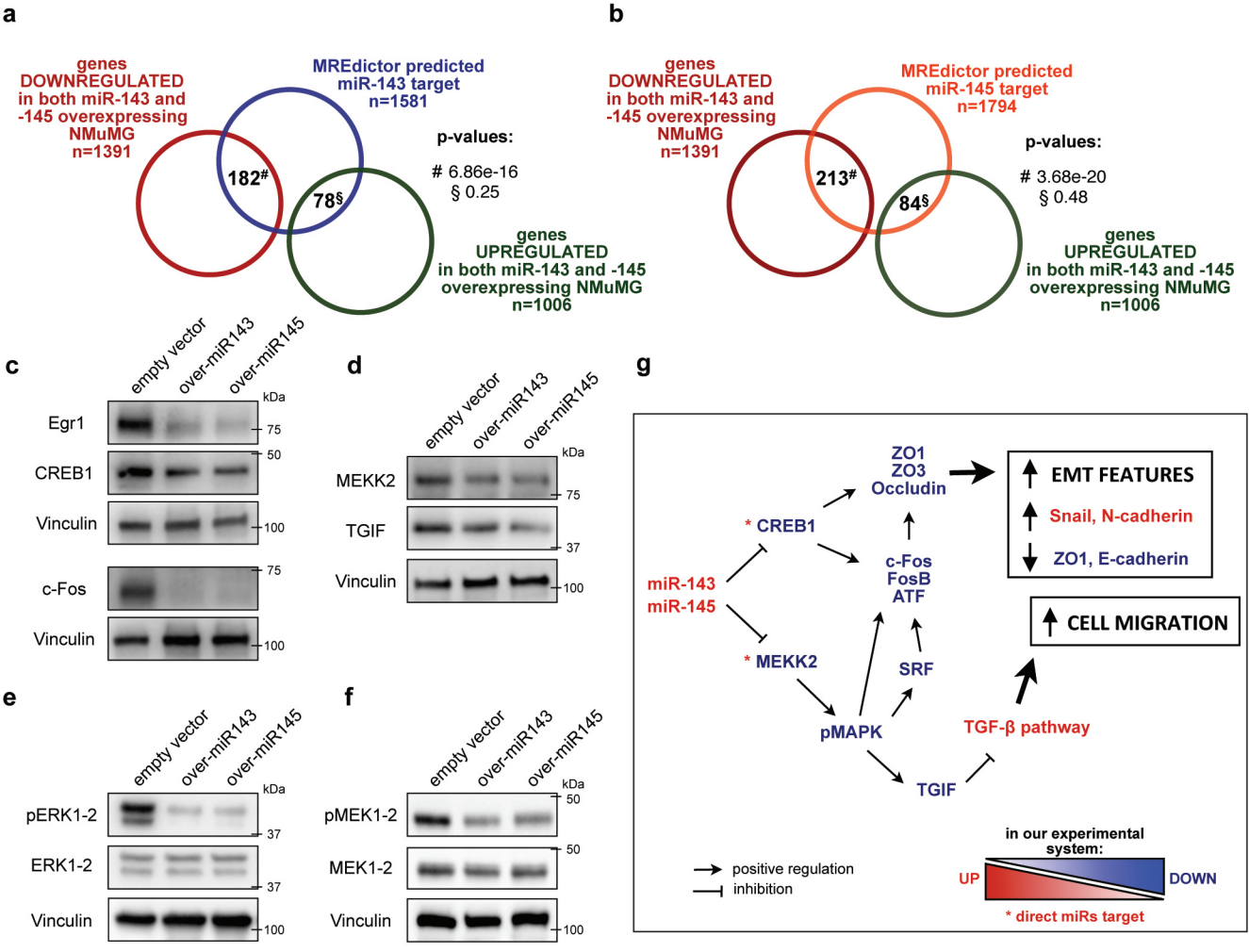
a
genes DOWNREGULATED in both miR-143 and -145 overexpressing NMuMG n=1391
MREdictor predicted miR-143 target n=1581
182#
78§
p-values:
6.86e-16
§ 0.25
genes UPREGULATED in both miR-143 and -145 overexpressing NMuMG n=1006
b
genes DOWNREGULATED in both miR-143 and -145 overexpressing NMuMG n=1391
MREdictor predicted miR-145 target n=1794
213#
84§
p-values:
3.68e-20
§ 0.48
genes UPREGULATED in both miR-143 and -145 overexpressing NMuMG n=1006
c
empty vector
over-miR143
over-miR145
kDa
Egr1
75
CREB1
50
Vinculin
100
c-Fos
75
Vinculin
100
d
empty vector
over-miR143
over-miR145
kDa
MEKK2
75
TGIF
37
Vinculin
100
e
empty vector
over-miR143
over-miR145
kDa
pERK1-2
37
ERK1-2
37
Vinculin
100
f
empty vector
over-miR143
over-miR145
kDa
pMEK1-2
50
MEK1-2
50
Vinculin
100
g
miR-143
miR-145
* CREB1
* MEKK2
ZO1
ZO3
Occludin
c-Fos
FosB
ATF
SRF
pMAPK
TGIF
TGF-β pathway
EMT FEATURES
Snail, N-cadherin
ZO1, E-cadherin
CELL MIGRATION
positive regulation
inhibition
in our experimental system:
UP
DOWN
* direct miRs target

SUPPLEMENTARY INFORMATION

Supplementary Fig.S1

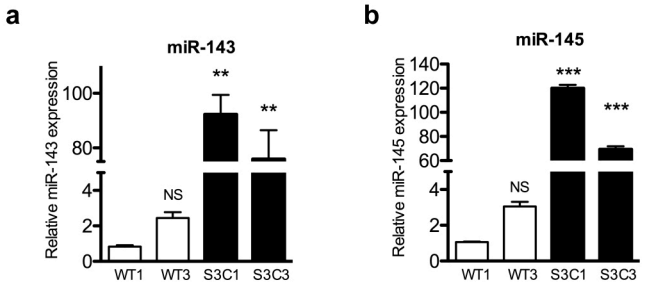

Supplementary Figure 1. miRNAs-143 and -145 expression levels in WT and S3C NeuT derived cell lines. a-b) miRNA expression levels were measured by qRT-PCR in two independent cell lines derived from WT and S3C NeuT tumors (WT1, WT3, S3C1, S3C3). Data are mean ± S.E.M. of expression values relative to WT1 cells. N=3.

Supplementary Fig.S2

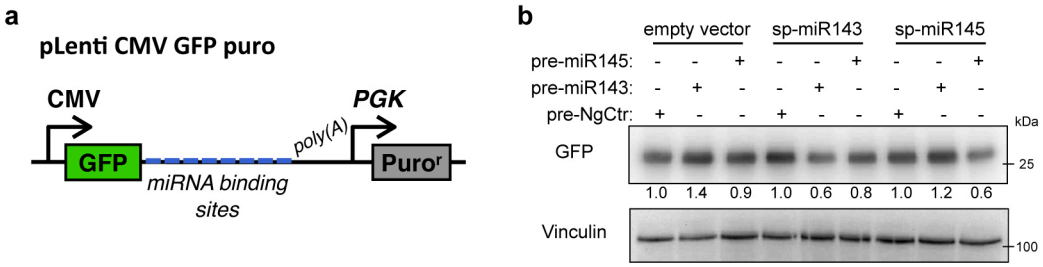

Supplementary Figure 2. Generation and testing of microRNAs sponge vectors. a) Schematic representation of pLenti CMV GFP Puro construct carrying multimerized miR-143 or miR-145 binding sites in the GFP gene 3'UTR. **b)** HEK293 cells were transiently transfected with sponge vectors specific for miR-143 (sp-miR143), miR-145 (sp-miR145) or an empty vector, together with the indicated miRNA precursors. GFP expression levels were measured by Western blot on total cell lysates. Numbers below the lanes indicate the densitometric analysis of the GFP band, normalized to Vinculin and relative to the values obtained with empty vector transfected cells.

Supplementary Fig.S3

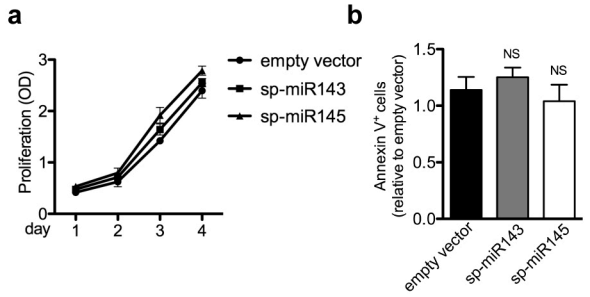

Supplementary Figure 3. Characterization of S3C cells transduced with the miR-143 or miR-145 sponge vectors. a) Proliferation of S3C cells stably transduced with the indicated sponge vectors was assessed for four days after plating, by measuring the Optical Density (OD) of Crystal violet-stained cells after solubilization in acetic acid. Results are shown as mean OD ± S.E.M. of three independent experiments performed in triplicate. N=3. **b)** Annexin V positive cells were measured by flow-cytometry upon 24h of plating on poly-HEMA treated dishes. Results are expressed as mean ± S.E.M. of Annexin V^+ cells from three independent experiments, relative to empty vector control cells. N=3.

Supplementary Fig.S4

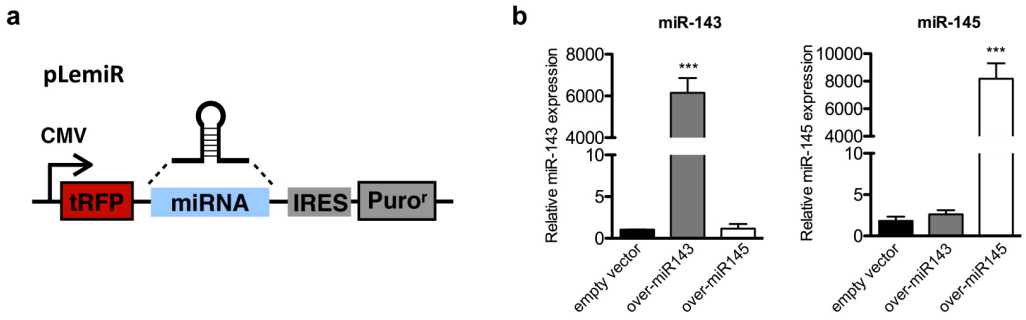

Supplementary Figure 4. Generation and testing of microRNAs overexpressing vectors. a) Schematic representation of the lentiviral vector pLemir, engineered to express the precursor sequences of either miR-143 or miR-145. **b)** Expression levels of the indicated miRNAs were evaluated by qRT-PCR in NMuMG cells transduced with the indicated overexpressing vectors or with the empty control vector. Results are shown as mean ± S.E.M. of expression values relative to empty vector control. N=3.

Supplementary Fig.S5

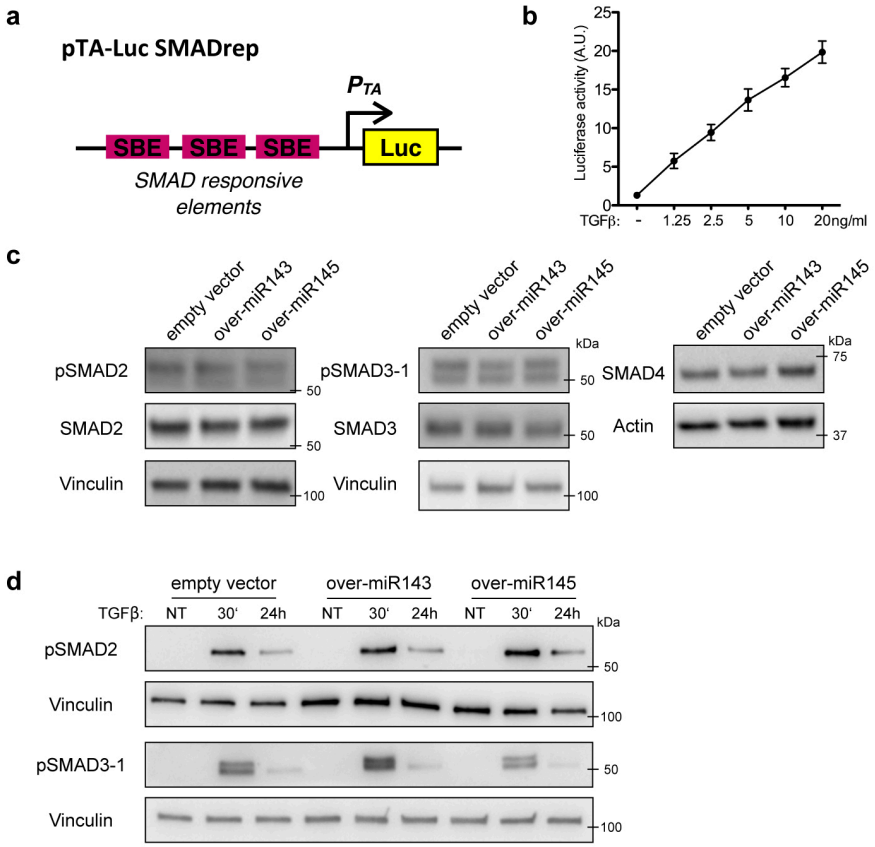

Supplementary Figure 5. Generation of the SMAD reporter vector and SMADs activity in NMuMG overexpressing cells. a) Schematic representation of the SMAD-reporter vector, where three SMAD binding elements (SBE) were inserted upstream of the minimal TK promoter in the pTA-Luciferase vector. **b)** Luciferase activity of NMuMG cells transfected with the SMAD-reporter vector and stimulated for 24h with the indicated doses of TGF-β. Results are shown as mean ± S.E.M. of luciferase values after normalization to Renilla luciferase and relative to untreated cells. **c)** Western blot assessing phosphorylated and total protein levels of the indicated SMAD proteins in NMuMG overexpressing cells under basal conditions. **d)** Western blot assessing phosphorylation levels of the indicated SMAD proteins in NMuMG overexpressing cells upon treatment with 10ng/ml TGF-β for the indicated time.

Supplementary Fig.S6

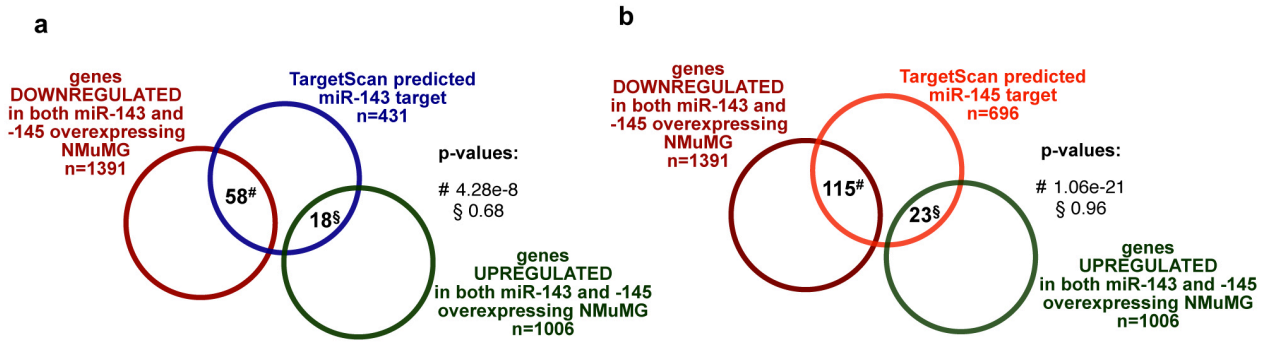

Supplementary Figure 6. TargetScan predicted miRNAs target are significantly enriched in dowregulated mRNAs. The Venn diagrams represent statistically significant enrichment of TargetScan predicted targets of miR-143 **(a)** or miR-145 **(b)** among the genes commonly downregulated by overexpression of either miRNA in NMuMG cells.

Supplementary Fig.S7

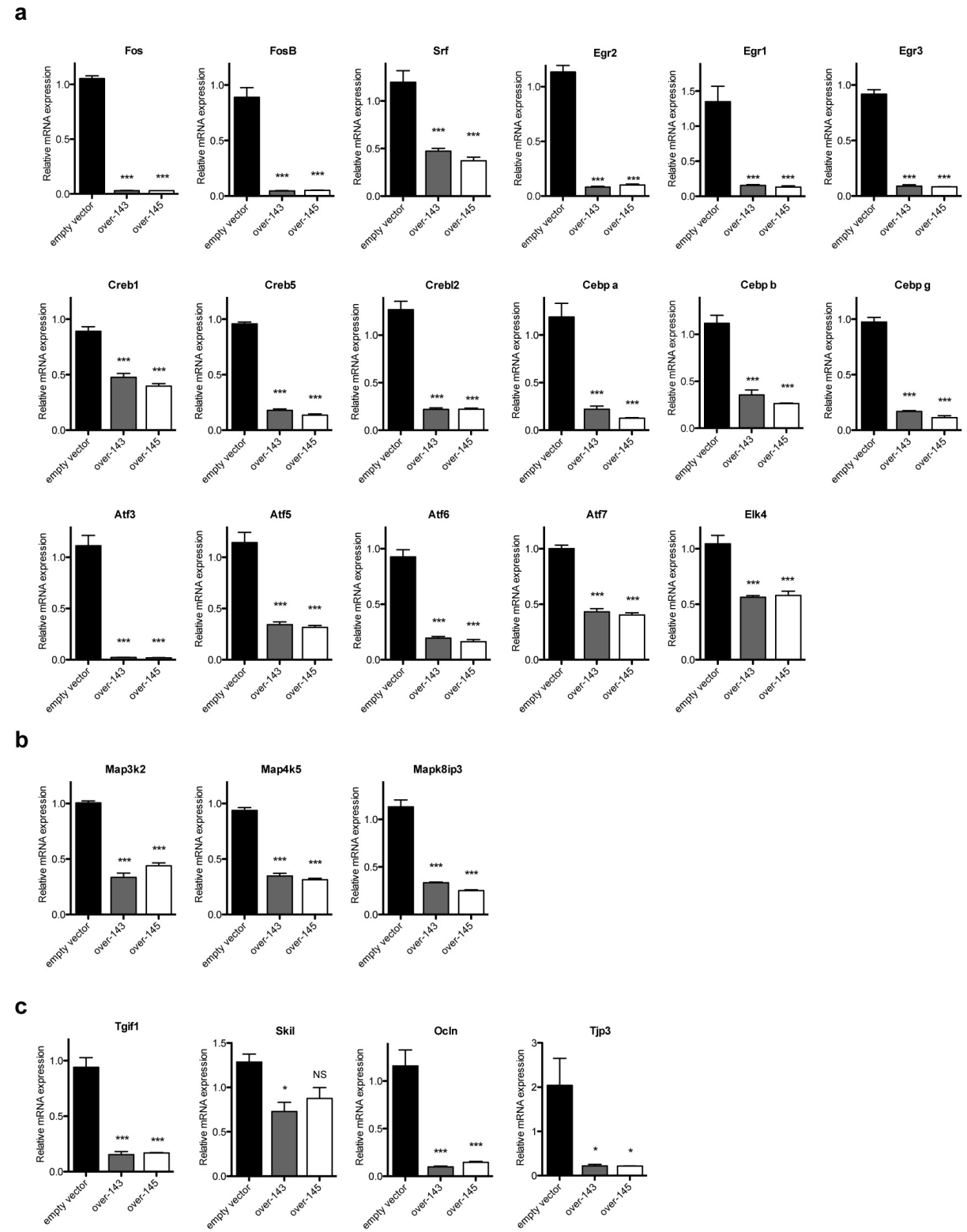

Supplementary Figure 7. qRT-PCR validation of RNA sequencing data. The expression of a subset of mRNAs identified as down-modulated by RNA sequencing was validated by qRT-PCR. The indicated mRNAs were measured from total RNA of the indicated NMuMG cells. The mRNA encoding for **(a)** Transcription factors, **(b)** MAP kinases, **(c)** TGFβ inhibitors and tight junction proteins were analyzed. Results are shown as mean ± S.E.M. of expression values relative to empty vector, after normalization to beta-actin RNA. *=P<0.05, **=P<0.01;***=P<0.001, N=4.